Step-by-Step Fracture of Two-Layer Stacked Graphene Membranes

Qing-Yuan Lin,[†,∥] Yi-Hang Zeng,[†,∥] Dameng Liu,[‡] Guang Yin Jing,[§] Zhi-Min Liao,[*,†,⊥] and Dapeng Yu[*,†,⊥]

[†]State Key Laboratory for Mesoscopic Physics, Department of Physics, Peking University, Beijing 100871, China, [‡]State Key Laboratory of Tribology, Tsinghua University, Beijing 100084, China, [§]National Key Laboratory and Incubation Base of Photoelectric Technology and Functional Materials, School of Physics, Northwest University, Xi'an 710069, China, and [⊥]Collaborative Innovation Center of Quantum Matter, Beijing, China. [∥]These authors contributed equally to this work.

ABSTRACT

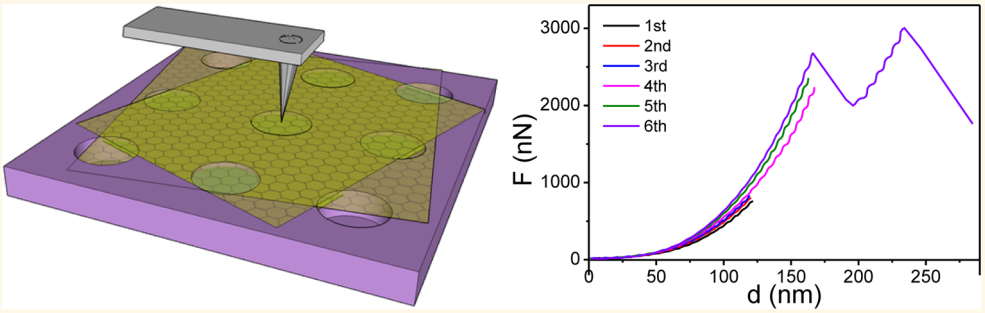

Layer-by-layer assembly of graphene has been proven to be an effective way to improve its mechanical properties, but its fracture mechanism, which is crucial for practical device applications, is still not clear and has not been fully studied yet. By consecutive stacking of two graphene monolayers, we fabricate two-layer stacked graphene membranes with a clean interface between the two layers. Fracture behavior of the two-layer stacked graphene membranes is studied using nanoindentation performed by atomic force microscopy. It is found that the fracture force distribution of stacked graphene is very different from that of monolayer graphene. Weibull statistics of fracture forces show that after layer-by-layer stacking of graphene, the membrane becomes less sensitive to the defects during nanoindentation, improving the overall performance of the graphene membranes. Interestingly, a third of our tested membranes show a stepwise fracture, which could serve as a warning message for the mechanical failure of multilayer graphene devices. Our study provides insight into the fracture mechanism of multilayer graphene membranes.

KEYWORDS: nanoindentation · Young's modulus · fracture force · two-layer stacked graphene

Graphene has generated a great deal of interest due to a wide range of unique physical properties.[1−4] In order to realize its potential applications, the mechanical properties of graphene need to be fully understood. Nanoindentation experiments, which are able to assess the intrinsic strength of graphene, have proved graphene to be the strongest material in the world.[5] Mechanically exfoliated graphene possesses excellent mechanical properties but has limited application due to the small size of the film. Chemical vapor deposition (CVD) is now commonly used to produce large-scale high-quality monolayer graphene (MG) films,[6−9] but subsequent experiments with CVD graphene show that wrinkles effectively lower the stiffness.[10] Besides, other defects such as grain boundaries,[11−21] Stone−Wales defects (pentagon−heptagon defects),[12,22] and voids[10] reduce the breaking strength of a MG film. Our previous experiments reveal that stretching leads to release of the wrinkles and a concomitant increase of the stiffness of CVD graphene.[23] Although the mechanical properties of MG have been widely investigated, the mechanical properties of stacked graphene monolayers still remain unknown. Layer-by-layer stacking of graphene monolayers allows the layered materials to be fabricated for versatile applications.[24] This method shows great potential in future device design in recent studies for its portability and reliability,[24,25] providing a convenient way to build a bottom-up graphene structure. This stack-like multilayer film is expected to improve mechanical properties as it can sustain larger mechanical loading before the failure. On the

* Address correspondence to liaozm@pku.edu.cn, yudp@pku.edu.cn.

Received for review June 23, 2014 and accepted September 25, 2014.

Published online September 25, 2014
10.1021/nn5033888

other hand, how the interaction between layers will affect the mechanical properties of the graphene stack is still unknown.[26,27] Moreover, more works are required to understand whether the fracture behavior of the stacked graphene structure will be the same as an individual monolayer. All of these problems need to be studied in detail to fully understand the fracture mechanism. A thorough study of the mechanical properties of the two-layer stacked graphene (TSG) membrane is crucial for the application of a layer-by-layer stacked graphene structure.

In this work, we report the mechanical properties of TSG membranes, which show very distinct fracture behavior compared to that of MG. By simply stacking two single layers of CVD graphene together, the percentage of membranes with premature fracture is greatly reduced compared to the monolayer. Only 11% (5 out of 44) of the tested TSG membranes have a fracture force less than half of the mean value, while for MG, this percentage is 44% (24 out of 54). The mean value of the fracture force of the TSG membranes is twice that of MG, which greatly improves the overall reliability of the TSG membranes. In addition, one-third of the tested TSG membranes show a step-by-step fracture behavior. Instead of the whole TSG membrane fracturing at one time, one graphene layer fractures at first, followed by the fracture of the second layer and the collapse of the whole membrane. This kind of fracture is a result of interlayer interaction, which can be explained by introducing a tape-like local mechanical interaction. Our study reveals a new fracture mechanism for layered two-dimensional materials, which will be helpful in guiding the design of devices based on layered structures.

RESULTS AND DISCUSSION

The TSG membranes were fabricated from layer-by-layer stacking of monolayer CVD graphene without involving any poly(methyl methacrylate) (PMMA) between the graphene layers. Details of the stacking procedure are described in the Materials and Methods section. The Raman spectrum (Supporting Information, Figure S1) of the TSG membrane shows the intensity ratio of the G peak to 2D peak is ~1:2, which is similar to that of MG, indicating negligible change of the band structure caused by interlayer interaction. The free-standing TSG membranes were fabricated by transferring the TSG membranes onto a Si substrate with arrays of circular holes using PMMA as the carrier. PMMA was later dissolved using acetone. The scanning electron microscope (SEM) image (Supporting Information, Figure S2) shows a high yield of the suspended TSG membranes after this transfer procedure.

An atomic force microscope (AFM) image of a TSG membrane is shown in Figure 1a. Nanoindentation was employed to carry out mechanical tests,[5] as illustrated in Figure 1b. A revised numerical method proposed in our previous work was used to describe the force–displacement curve properly.[23] We found that manual selection of the zero force–displacement point (ZDP) largely affects the fitting result of Young's modulus; therefore, we developed a revised numerical method to determine this point more precisely. Basically, the solution is to avoid the manual decision of the zero point and use the curve itself to deduce this point. We treated the zero point as an unknown parameter of the curve in the fitting equation. The result turns out that Young's modulus is much less sensitive to the selection of the starting point of the curve used to fit the data. In other words, our revised method can avoid the tricky definition of ZDP and make it easier and more accurate to acquire the Young's modulus. After measuring the elastic properties of each TSG membrane, we applied a large load to fracture the membrane and recorded its fracture behavior. A typical fractured membrane after nanoindentation is shown in Figure 1c,d by AFM and SEM, respectively. In our experiments, the interlayer slip of the TSG membrane is not observed. Because the interface may be complicated due to possible roughness, grain boundaries, and ripples, it is very likely that the complicated interlayer interaction prevents interlayer sliding in our TSG membranes. On the other hand, the vertical deformation of the TSG membrane at the center is on the order of ~100 nm, the diameter of the membrane is 2.2 μm, and the thickness of the TSG membrane is ~1 nm. Therefore, the strain difference between the two layers can be negligible, and the shear stress would be very small, resulting in the absence of an interlayer slip.

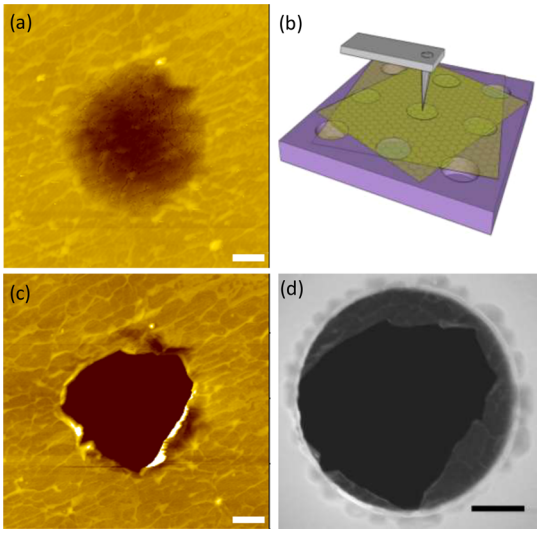

Figure 1. (a) AFM image of a typical TSG membrane suspended on a hole on a Si substrate. (b) Schematic diagram of the TSG membrane measured by nanoindentation using AFM. (c) AFM image and (d) SEM image of the same TSG membrane after fracture. The hole is 2.2 μm in diameter. The scale bars are 500 nm.

Typical force–displacement curves for a single-layer graphene and a TSG membrane are shown in Figure 2. Using the revised numerical method, the mechanical

properties of 44 tested TSG membranes were recorded and are shown in Figure 3. We can obtain a 2D Young's modulus from the fitting of the experimental data. To compare with bulk materials, the 3D Young's modulus can be calculated through the 2D value divided by thickness of the membrane, using a nominal value of h = 0.335 nm as the thickness of MG and a doubled value h = 0.67 nm for TSG.[5] Extracted from the data presented in Figure 3a,b, it is found that the average Young's modulus (435 GPa) of the TSG membranes is very close to that of MG (423 GPa) in our experiments. The average fracture force was doubled from 1094 nN for MG to 2408 nN for the TSG membranes, according to the data presented in Figure 3c,d. In addition, the in-plane stresses at fracture for MG and TSG are also calculated (Supporting Information, Figure S3). The average breaking stress for MG is 9.6 N/m, while for TSG, it is 21.1 N/m. It is worth noting that the details of the overall mechanical behaviors of the TSG membranes are very different from that of MG. Both the Young's moduli and fracture forces of the MG membranes are seriously deviated from Gaussian distributions (Figure 3a,c). On the contrary, the statistics of both Young's moduli (Figure 3b) and fracture forces (Figure 3d) of the TSG membranes present a nice Gaussian distribution, indicating that the interlayer interaction plays an important role on the mechanical behavior of the TSG membranes. Moreover, the interaction between the two layers makes the probability distribution of the fracture force of the TSG deviate from the square of that of MG.

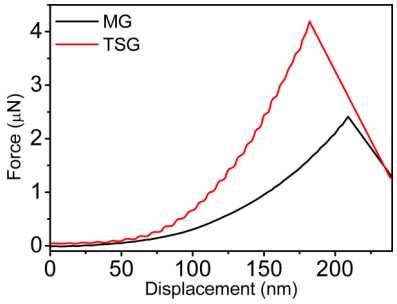

Figure 2. Force−displacement curves of monolayer graphene and two-layer stacked graphene membranes.

We can roughly separate our MG membranes into two categories based on their mechanical behavior due to strength difference. The low-strength category fractured in the first or second indentation test under a small load, whereas the high-strength one was able to hold multiple indentations and large loading forces. The weaker membranes have lower stiffness and smaller fracture force and hence are more fragile than the other. It is reported that there are two kinds of grain boundaries (GBs) in CVD graphene, the well-stitched GB and the overlapped GB; the former one has high strength, whereas the latter one is much weaker.[28] Therefore, the two types of grain boundaries are potentially responsible for our observations of the two strength levels of MG.

For the TSG membranes, we can no longer see two categories of membranes; instead, it only shows a single Gaussian distribution. The Weibull distribution was used to further analyze the results. The Weibull probability distribution is described as $P = 1 - \exp[-(F_f/F_0)^m]$, where P is the cumulative probability of fracture at a fixed force F_f, F_0 is a constant force, and m is the Weibull modulus reflecting the distribution breadth.[5] A large value of m suggests a narrow variation in breaking force, which indicates a narrow range of defects or that the failure mode is less sensitive to the defects.[5] We plot the two-parameter Weibull probability distribution in Supporting Information Figure S4. The fittings by Weibull probability distribution give the parameters of m = 1.13,

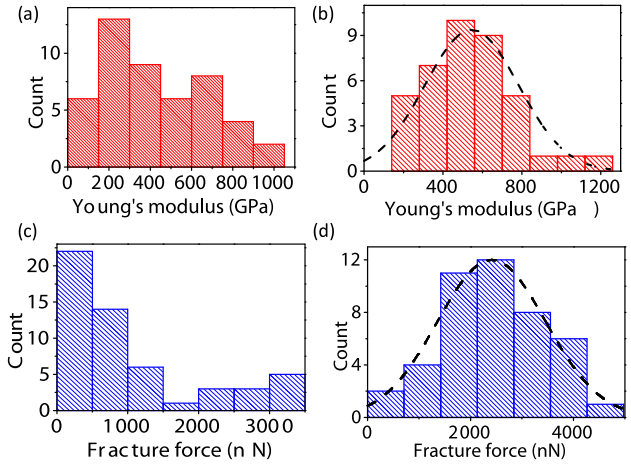

Figure 3. Histograms of mechanical properties of MG (a,c) and TSG (b,d) membranes. (a,b) Young's modulus distribution with an average of 423 and 435 GPa for the MG and TSG membranes, respectively. (c,d) Fracture force distribution with an average fracture force of 1094 and 2408 nN for the MG and TSG membranes, respectively. The dashed lines in (b) and (d) show the fit of the Gaussian distribution to the data.

F_0 = 1064.2 nN for MG and m = 2.31, F_0 = 2740.8 nN for TSG. The large value of m of TSG indicates that the TSG has an improved fracture behavior compared to MG, which suggests that the TSG is less sensitive to the defects considering that MG and TSG should have similar defect density.

According to Figure 3c,d, the TSG has on average much higher fracture forces than that of MG. The improvement in failure behavior of the TSG can be explained by considering interlayer interaction between two graphene layers while stacked together. For monolayer CVD graphene, a line defect (*i.e.*, grain boundary) could easily initiate a crack while a load is applied on this defect by local stress concentration,[10] and it will propagate and fracture the entire membrane once the crack is formed. Therefore, the MG is more fragile because the tip has a larger chance to indent on defects. However, if we stack two layers of graphene together, the chance of two line defects having the same location becomes very small. Since the TSG membrane only fractures easily when the tip is directly indented at a place where both membranes have line defects overlapping, the failure probability of TSG will be much smaller than that of MG. For any line defect in one of the graphene layers, the other layer will act as a protecting layer to avoid easy fracture of the stacked membrane. We also observed stiffness enhancement behavior in the TSG membranes by sequential indentations, as shown in Figure 4. The Young's modulus of ~610 GPa calculated from the curve obtained in the first indentation is increased to 865 GPa for the sixth indentation. The stiffness enhancement is attributed to the stretch-induced flatness of the wrinkles during the loading process, which agrees well with our previous Young's modulus enhancement for individual graphene monolayers.[23]

Importantly, the fracture behavior of the TSG membrane is very different from that of MG. For 15 out of 44 tested TSG membranes, they showed two separate fracture points during the loading process. Figure 5a shows a typical force–displacement curve for the fracture behavior, and each sudden decrease of force in the force–displacement curve represents a fracture. Here F_1 is defined as the first fracture force, and F_2 is defined as the force where the load starts to grow again after the first fracture. Intuitively, the value of F_2 is smaller than that of F_1 since the fracture releases the accumulating stress by indentation. The F_3 is defined as the second fracture force after the first fracture. Note that the second fracture can happen in two cases: one is the successive fracture after the first fracture, as shown in Figure 5a, and the other is the fracture occurring at the second round of indentation after the first fracture of the membrane, which requires that there is no further fracture during the first indentation after first fracture, as shown in Figure 5b. It is naturally inferred that the two-step fracture can only occur in

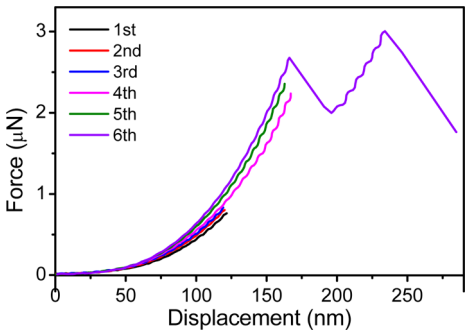

Figure 4. Stiffness enhancement of a typical TSG membrane. The Young's modulus of this sample was increased from 610 to 865 GPa during indentation cycles. Two separate fracture points were also found in this sample.

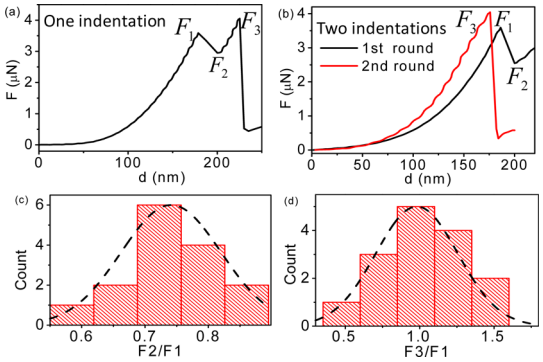

Figure 5. Force–displacement curves of a TSG membrane showing two separate fractures (a) in one indentation and (b) in two indentations. F_1, F_2, and F_3 are defined as the first fracture force, the smaller force where the load starts to grow again after the first fracture, and the second fracture force, respectively. (c,d) Histograms of ratios of F_2/F_1 and F_3/F_1, respectively. The dashed lines in graphs (c) and (d) show the fit of Gaussian distribution to the data.

the membranes where both of the two layers of graphene are strong enough. After one graphene layer is fractured, the other layer should be strong enough to sustain that stress. The fact that the 44% of the tested MG membranes have a fracture force less than half of the mean value would be the most limiting factor for only having 1/3 of the TSG membranes with step-by-step fracture.

It is shown that sequential indentations may enhance the Young's modulus of the membrane, which is attributed to the stretch-induced flatness of the wrinkles during the loading process.[23] On the other hand, it is unlikely that the defect structure and distribution changed during this process. Since the fracture force depends on the strength of the defects, we believe that the fracture forces should not be much different whether the membrane is fractured in one indentation or two indentations. In other words, the fracture forces of F_1, F_2, and F_3 were considered regardless of the indentation times. In order to discuss the TSG fracture mechanism, we introduce the ratios of F_2/F_1 and F_3/F_1 and plot the diagram for the 15 step-by-step fractures. As shown in Figure 5c,d, we found a Gaussian-like

distribution of F_2/F_1 and F_3/F_1 with average values of 0.74 and 0.98, respectively.

Here, the values of F_2/F_1 reflect the relaxation of the membrane after releasing the stress during the first fracture. The F_2/F_1 with an average value of 0.74 indicates that the TSG system has a notable self-adjusting ability *via* releasing local stress. The F_3/F_1 is the ratio of the first and second fracture force. If the two layers have no interlayer interaction, the force loaded on each independent monolayer should be one-half of F_1 at the first fracture because there are two layers to sustain the stress before the first fracture; for the second fracture, there is only one layer to sustain the stress, and the second fracture force F_3 should be roughly one-half of F_1 considering the similar strength of the two graphene layers. Therefore, the experimental observation of $F_3/F_1 \sim 0.98$ suggests the strong interlayer interaction of the TSG. The first fracture is a local fracture, which releases the local stress. Then, the strong interaction makes the two layers stick firmly, thus preventing the fracture propagation and the rupture of the whole membrane. One important fact about the step-by-step fracture is that all of these membranes with two separate fractures have relatively large fracture forces. Hence we assume that step-by-step fracture will only occur when the GBs are not very weak and they are not overlapped with each other. After the first fracture, the surviving graphene layer should be strong enough to endure the stress. Moreover, the strong interaction makes the two layers attach together, with the first fractured graphene layer acting like an adhesive "tape", so that this structure can undertake the stress by the two graphene layers together even after the first fracture. As the membrane is loaded further, the second fracture condition will be similar to that of the first fracture, which results in the ratio of $F_3/F_1 \sim 1$.

CONCLUSIONS

In conclusion, we have studied the mechanical properties of suspended two-layer stacked graphene membranes. By randomly stacking two monolayers of CVD graphene together, the membranes become much less fragile. Step-by-step fracture of TSG membranes was observed with two close fracture forces on average, which is ascribed to the first broken layer still undergoing a pressing force applied by the tip. This step-by-step fracture behavior has the implication of a warning message for the mechanical failure of the multilayer graphene devices. Our study reveals a new fracture mechanism of stacked two-dimensional materials, and such a finding will be particularly helpful while designing devices based on graphene,[2,29−31] MoS_2,[32] *etc.*

MATERIALS AND METHODS

Fabrication of Suspended TSG Membranes. Two-layer stacked graphene membranes were fabricated through layer-by-layer stacking of monolayer CVD graphene.[33] Monolayer graphene was grown on copper foil.[34] Then a thin layer of poly(methyl methacrylate) (PMMA) was spin-coated onto one side of the copper foil. The copper foil was then etched away in ferric chloride aqueous solution, and the graphene/PMMA film floated on the top of the solution. After the graphene/PMMA film was rinsed in deionized water three times, another copper foil with MG was used to stack with the graphene/PMMA film. After the films were dried in air for several hours to ensure the two graphene layers adhere tightly, we used the same method to etch the copper foil and rinse the membrane.[35] Then the graphene/graphene/PMMA film was fished out using the silicon substrate with arrays of circular holes. PMMA was later dissolved using acetone. Instead of directly pulling the samples out of acetone, we used a small box to take the substrate out of the acetone and put it into isopropyl alcohol, which allowed the substrate to be immersed in the solution during the procedure. This method prevented damage due to surface tension while drying in acetone and resulted in a high yield of freestanding TSG membranes on the circular holes on a silicon substrate.

Measurement of Mechanical Properties. Nanoindentation was employed to carry out mechanical tests,[5] and a revised numerical method proposed in our previous work was used to describe the force curve properly.[23] During nanoindentation, the measured deformation distance includes both the displacement of the membrane and the deflection of the cantilever. For calibration of the force−displacement curve, we first performed nanoindentation on a silicon substrate to acquire the relationship between force and cantilever deflection to eliminate the influence of cantilever deflection. The relationship between the force f and the vertical position of the tip relative to the substrate Z was described by $f = (f_0 - k_1\delta_0 - k_2\delta_0^3) + (k_1 + 3k_2\delta_0^2)Z - (3k_2\delta_0)Z^2 + k_2Z^3$, where $k_1 = \sigma_0^{2D}\pi$, $k_2 = E^{2D}q^3/a^2$, $\delta = Z - \delta_0$ is the displacement of the membrane at the center, q is a constant, a is the radius of the hole, and δ_0 is the zero-displacement point. The force−displacement curve was fitted to obtain the 2D Young's modulus E^{2D} from the parameter k_2. The fracture force was calculated as $f - f_0$, where f was obtained when the force suddenly decreased with displacement. After obtaining elastic properties of each TSG membrane, we applied a large load to fracture the membrane and recorded its fracture behavior.

Conflict of Interest: The authors declare no competing financial interest.

Acknowledgment. This work was supported by MOST (Nos. 2013CB934600, 2013CB932602), National Nature Science Foundation of China (NSFC) (Nos. 11274014, 11234001, 51105222), and the Program for New Century Excellent Talents in University of China (No. NCET-12-0002). Y.H.Z. and Q.Y.L. were supported by the President's Fund for Undergraduate Research of Peking University.

Supporting Information Available: More details on Raman characterization, SEM image of the TSG membranes, calculation of in-plane stress, fitting with Weibull distribution. This material is available free of charge *via* the Internet at http://pubs.acs.org.

REFERENCES AND NOTES

1. Novoselov, K. S.; Fal'ko, V. I.; Colombo, L.; Gellert, P. R.; Schwab, M. G.; Kim, K. A Roadmap for Graphene. *Nature* **2012**, *490*, 192–200.
2. Xia, F. N.; Farmer, D. B.; Lin, Y. M.; Avouris, P. Graphene Field-Effect Transistors with High On/Off Current Ratio and Large Transport Band Gap at Room Temperature. *Nano Lett.* **2010**, *10*, 715–718.
3. Liu, M.; Yin, X.; Ulin-Avila, E.; Geng, B.; Zentgraf, T.; Ju, L.; Wang, F.; Zhang, X. A Graphene-Based Broadband Optical Modulator. *Nature* **2011**, *474*, 64–67.

4. Ju, L.; Geng, B.; Horng, J.; Girit, C.; Martin, M.; Hao, Z.; Bechtel, H. A.; Liang, X.; Zettl, A.; Shen, Y. R.; *et al.* Graphene Plasmonics for Tunable Terahertz Metamaterials. *Nat. Nanotechnol.* **2011**, *6*, 630–634.
5. Lee, C.; Wei, X.; Kysar, J. W.; Hone, J. Measurement of the Elastic Properties and Intrinsic Strength of Monolayer Graphene. *Science* **2008**, *321*, 385–388.
6. Li, X.; Cai, W.; An, J.; Kim, S.; Nah, J.; Yang, D.; Piner, R.; Velamakanni, A.; Jung, I.; Tutuc, E.; *et al.* Large-Area Synthesis of High-Quality and Uniform Graphene Films on Copper Foils. *Science* **2009**, *324*, 1312–1314.
7. Bae, S.; Kim, H.; Lee, Y.; Xu, X.; Park, J.-S.; Zheng, Y.; Balakrishnan, J.; Lei, T.; Kim, H. R.; Song, Y. I.; *et al.* Roll-to-Roll Production of 30-Inch Graphene Films for Transparent Electrodes. *Nat. Nanotechnol.* **2010**, *5*, 574–578.
8. Petrone, N.; Dean, C. R.; Meric, I.; van der Zande, A. M.; Huang, P. Y.; Wang, L.; Muller, D.; Shepard, K. L.; Hone, J. Chemical Vapor Deposition-Derived Graphene with Electrical Performance of Exfoliated Graphene. *Nano Lett.* **2012**, *12*, 2751–2756.
9. Lee, S.; Lee, K.; Zhong, Z. H. Wafer Scale Homogeneous Bilayer Graphene Films by Chemical Vapor Deposition. *Nano Lett.* **2010**, *10*, 4702–4707.
10. Ruiz-Vargas, C. S.; Zhuang, H. L.; Huang, P. Y.; van der Zande, A. M.; Garg, S.; McEuen, P. L.; Muller, D. A.; Hennig, R. G.; Park, J. Softened Elastic Response and Unzipping in Chemical Vapor Deposition Graphene Membranes. *Nano Lett.* **2011**, *11*, 2259–2263.
11. Zhang, J.; Zhao, J.; Lu, J. Intrinsic Strength and Failure Behaviors of Graphene Grain Boundaries. *ACS Nano* **2012**, *6*, 2704–2711.
12. Wei, Y.; Wu, J.; Yin, H.; Shi, X.; Yang, R.; Dresselhaus, M. The Nature of Strength Enhancement and Weakening by Pentagon−Heptagon Defects in Graphene. *Nat. Mater.* **2012**, *11*, 759–763.
13. Wang, B.; Puzyrev, Y.; Pantelides, S. T. Strain Enhanced Defect Reactivity at Grain Boundaries in Polycrystalline Graphene. *Carbon* **2011**, *49*, 3983–3988.
14. Cao, A. J.; Yuan, Y. T. Atomistic Study on the Strength of Symmetric Tilt Grain Boundaries in Graphene. *Appl. Phys. Lett.* **2012**, *100*, 211912.
15. Grantab, R.; Shenoy, V. B.; Ruoff, R. S. Anomalous Strength Characteristics of Tilt Grain Boundaries in Graphene. *Science* **2010**, *330*, 946–948.
16. Huang, P. Y.; Ruiz-Vargas, C. S.; van der Zande, A. M.; Whitney, W. S.; Levendorf, M. P.; Kevek, J. W.; Garg, S.; Alden, J. S.; Hustedt, C. J.; Zhu, Y.; *et al.* Grains and Grain Boundaries in Single-Layer Graphene Atomic Patchwork Quilts. *Nature* **2011**, *469*, 389–392.
17. Liu, T.-H.; Pao, C.-W.; Chang, C.-C. Effects of Dislocation Densities and Distributions on Graphene Grain Boundary Failure Strengths from Atomistic Simulations. *Carbon* **2012**, *50*, 3465–3472.
18. Wu, J. T.; Wei, Y. J. Grain Misorientation and Grain-Boundary Rotation Dependent Mechanical Properties in Polycrystalline Graphene. *J. Mech. Phys. Solids* **2013**, *61*, 1421–1432.
19. Zhang, J. F.; Zhao, J. J. Mechanical Properties of Bilayer Graphene with Twist and Grain Boundaries. *J. Appl. Phys.* **2013**, *113*, 043514.
20. Carlsson, J. M.; Ghiringhelli, L. M.; Fasolino, A. Theory and Hierarchical Calculations of the Structure and Energetics of [0001] Tilt Grain Boundaries in Graphene. *Phys. Rev. B* **2011**, *84*, 165423.
21. Malola, S.; Häkkinen, H.; Koskinen, P. Structural, Chemical, and Dynamical Trends in Graphene Grain Boundaries. *Phys. Rev. B* **2010**, *81*, 165447.
22. Chandra, N.; Namilae, S.; Shet, C. Local Elastic Properties of Carbon Nanotubes in the Presence of Stone−Wales Defects. *Phys. Rev. B* **2004**, *69*, 094101.
23. Lin, Q.-Y.; Jing, G.; Zhou, Y.-B.; Wang, Y.-F.; Meng, J.; Bie, Y.-Q.; Yu, D.-P.; Liao, Z.-M. Stretch-Induced Stiffness Enhancement of Graphene Grown by Chemical Vapor Deposition. *ACS Nano* **2013**, *7*, 1171–1177.
24. Yuk, J. M.; Kim, K.; Alemán, B. N.; Regan, W.; Ryu, J. H.; Park, J.; Ercius, P.; Lee, H. M.; Alivisatos, A. P.; Crommie, M. F.; *et al.* Graphene Veils and Sandwiches. *Nano Lett.* **2011**, *11*, 3290–3294.
25. Hwang, H.; Joo, P.; Kang, M. S.; Ahn, G.; Han, J. T.; Kim, B. S.; Cho, J. H. Highly Tunable Charge Transport in Layer-by-Layer Assembled Graphene Transistors. *ACS Nano* **2012**, *6*, 2432–2440.
26. Kim, K.; Coh, S.; Tan, L. Z.; Regan, W.; Yuk, J. M.; Chatterjee, E.; Crommie, M. F.; Cohen, M. L.; Louie, S. G.; Zettl, A. Raman Spectroscopy Study of Rotated Double-Layer Graphene: Misorientation-Angle Dependence of Electronic Structure. *Phys. Rev. Lett.* **2012**, *108*, 246103.
27. Kordkheili, S. A. H.; Moshrefzadeh-Sani, H. Mechanical Properties of Double-Layered Graphene Sheets. *Comput. Mater. Sci.* **2013**, *69*, 335–343.
28. Lee, G.-H.; Cooper, R. C.; An, S. J.; Lee, S.; van der Zande, A.; Petrone, N.; Hammerberg, A. G.; Lee, C.; Crawford, B.; Oliver, W.; *et al.* High-Strength Chemical-Vapor-Deposited Graphene and Grain Boundaries. *Science* **2013**, *340*, 1073–1076.
29. Zhang, Y. B.; Tang, T. T.; Girit, C.; Hao, Z.; Martin, M. C.; Zettl, A.; Crommie, M. F.; Shen, Y. R.; Wang, F. Direct Observation of a Widely Tunable Bandgap in Bilayer Graphene. *Nature* **2009**, *459*, 820–823.
30. Cai, W.; Zhu, Y.; Li, X.; Piner, R. D.; Ruoff, R. S. Large Area Few-Layer Graphene/Graphite Films as Transparent Thin Conducting Electrodes. *Appl. Phys. Lett.* **2009**, *95*, 123115.
31. Yu, W. J.; Liu, Y.; Zhou, H.; Yin, A.; Li, Z.; Huang, Y.; Duan, X. Highly Efficient Gate-Tunable Photocurrent Generation in Vertical Heterostructures of Layered Materials. *Nat. Nanotechnol.* **2013**, *8*, 952–958.
32. Lee, Y. H.; Zhang, X. Q.; Zhang, W. J.; Chang, M. T.; Lin, C. T.; Chang, K. D.; Yu, Y. C.; Wang, J. T. W.; Chang, C. S.; Li, L. J.; *et al.* Synthesis of Large-Area MoS_2 Atomic Layers with Chemical Vapor Deposition. *Adv. Mater.* **2012**, *24*, 2320–2325.
33. Chen, J. J.; Meng, J.; Zhou, Y. B.; Wu, H. C.; Bie, Y. Q.; Liao, Z. M.; Yu, D. P. Layer-by-Layer Assembly of Vertically Conducting Graphene Devices. *Nat. Commun.* **2013**, *4*, 1921.
34. Bie, Y.; Zhou, Y.; Liao, Z.; Yan, K.; Liu, S.; Zhao, Q.; Kumar, S.; Wu, H.; Duesberg, G. S.; Cross, G. L. W.; *et al.* Site-Specific Transfer-Printing of Individual Graphene Microscale Patterns to Arbitrary Surfaces. *Adv. Mater.* **2011**, *23*, 3938–3943.
35. Chen, J. J.; Meng, J.; Yu, D. P.; Liao, Z. M. Fabrication and Electrical Properties of Stacked Graphene Monolayers. *Sci. Rep.* **2014**, *4*, 5065.